

Print-Assisted Layer - by - Layer Fabrication of Mixed-Matrix Membrane for Gas Separation

Mohammed S. Al-Ajmi¹, Amna S. Al-Jabri¹, Jimoh K. Adewole^{1#}, Faisal R. AL Marzuqi¹, Habeebllah B. Oladipo¹

¹Department of Engineering (Process Engineering), International Maritime College, National University of Science & Technology, Oman.

#Advisor

ABSTRACT

The process intensification principles of optimizing the driving forces/resistances at every scale and the spatial domain were investigated using a print-assisted technique. The investigation was done by using a LaserJet printer to fabricate structured mixed-matrix membranes for gas separation. The physico-chemical properties of the fabricated membranes were evaluated using FTIR, and XRD. The microstructure of the membrane was evaluated using Scanning Electron Microscope (SEM) and optical microscope. The separation performance was evaluated using constant-pressure gas permeation test. The capability of the membrane to separate a mixture of two gases were tested using CO₂ and CH₄. The results from optical microscope analysis showed that membrane fabricated using print-assisted method possessed a well-structured morphology which can enhance the predictability of their performance. The gas permeations results showed that the transport mechanism of the membranes changed from Knudsen to molecular sieve as the number of print layers was increased from 0 to 7 layers. Overall, the fabricated membrane showed some potentials for separating CO₂/CH₄ mixture.

Introduction

Sustainable industrial growth is globally recognised as one of the current challenges that is facing the manufacturing sector. Process intensification (PI) is described as a design approach that offers solutions to these challenges. PI solutions can substantially lead to shrinking process equipment size, energy saving, costs reduction, increased safety, and reduced environmental impact (Reay, Ramshaw and Harvey, 2013a; Sitter, Chen and Grossmann, 2019). The application of best PI practices is based on four principles: maximizing effectiveness of intra & inter molecular events; giving each molecule same processing experience; optimizing the driving forces/resistances at every scale and maximizing the specific surface areas to which these forces /resistances apply; and maximizing the synergistic effect from partial processes (Reay, Ramshaw and Harvey, 2013b; Holtbruegge, Wierschem and Lutze, 2014; Stankiewicz, 2020). The optimization of driving forces is closely related to the transport rate across interfaces. On a general note, this principle, which refers to the need to maximize the overall effect, can be achieved by maximizing the specific surface area to which the driving force or resistance is applied. Furthermore, enhanced specific surface area can be realised via structuring the equipment or material used for the process (Stankiewicz and Moulijn, 2000; Stankiewicz, 2020).

PI can be achieved through the functional, spatial, thermodynamics and temporal domains (Stankiewicz, 2020). In the spatial domain, emphasis is laid on the need to avoid randomness in process equipment. For this reason, it is highly recommended to replace randomness in process equipment with structured ones. Unfortunately, a large number of process equipment exhibit randomness in one way or the other and at various scales (including meso and macro scales) (Reay, Ramshaw and Harvey, 2013b; Stankiewicz, 2020). Random character at any scale can reduce the efficiency, cause safety problems, reduce process predictability and ability to control process behaviour. One of

the major causes of randomness in process equipment or material is the manufacturing technique used for its production.

The use of innovative technologies such as membrane in achieving the goals of PI have received much more attention these days. Membrane is a sustainable technology that can substantially reduce the energy consumption in many industrial processes, reduce waste, make separation processes more cost-effective, safer, and sustainable (Drioli, Stankiewicz and Macedonio, 2011; Adewole and Ahmad, 2017). The technology has been investigated worldwide because it is best known to be a suitable technology for actualizing process intensification (Drioli, Stankiewicz and Macedonio, 2011). The heart of membrane equipment is the membrane material. In membrane-based gas separation, the membrane materials can be polymer (organic), inorganic or mixed-matrix (Adewole *et al.*, 2013). This paper therefore investigates the use of a print-assisted membrane preparation technique to fabricate mixed-matrix membrane material for gas separation. The physico-chemical properties of the fabricated mixed-matrix membranes were analysed using optical microscopy, FTIR, and XRD while the separation performance was evaluated using gas permeability and selectivity of methane (CH₄) and carbon dioxide (CO₂).

Methodology and Materials

The materials and equipment used in this research include laserjet printer, lignocellulosic paper-based support, gas permeation set-up and gases (CH₄ and CO₂).

Printing

Computer-aided design of flat sheet mixed-matrix membrane was carried out using a word processing software. The text fill was set to solid fill with black colour, transparency of 0% and width of 1pt. The text outline is of no line while the shadow was left as default. The Reflection transparency was set to 100%, while the size, blur and the distance were maintained at 0. The glow colour was set to black, and the size and transparency set to 0. The soft edges were left as default and not 3-D format was used. The textbox was vertically aligned to the middle, text direction to the horizontal. The text wrapping was set to in front of text. The absolute height was 10.72cm while the width was 10cm. The margins were set to 0.25cm (left and right), and 0.13cm (top and bottom). The printing was done using a laser jet printer.

Surface Morphology

The morphology of the fabricated membrane samples was studied using Scanning Electron Microscope and Optical microscope imaging. Digital Microscope USB X1000 RoHS was used to capture an optical image of the sample surfaces and cross-section.

X-ray Diffraction

X-ray diffraction (XRD) test was conducted on the membrane samples using a diffractometer with Cu Ka radiation of $k = 5$ 1.5406 Å, voltage of 40.0 kV and current of 30.0 mA. Samples were scanned from 10 to 60.

The crystallinity of the membrane was estimated from the XRD data using the equation below.

$$C_r I = \frac{I_{200} - I_{110}}{I_{200}} \times 100 \quad \text{Equation 1}$$

Where, $C_r I$ is the Crystallinity Index, I_{200} is the intensity of the cellulose crystalline peak and I_{110} is the intensity of the amorphous peak.

Separation Performance Measurement using Permeation Test

Gas permeability was measured by a constant pressure/variable volume apparatus. Detailed of this apparatus has been published elsewhere (Ahmad *et al.*, 2014). The apparatus is composed of the permeation cell and a gas flowmeter on the downstream side. At steady-state condition, gas permeability was calculated using the following equation:

$$P = \frac{22,414}{A} \frac{l}{(p_2 - p_1)} \frac{p_1}{RT} \frac{dV}{dt} \quad \text{Equation 2}$$

where A is the membrane area (cm^2), p_2 and p_1 are feed or upstream and permeate or downstream pressures, respectively, R is the universal gas constant ($6236.56 \text{ cm}^3 \text{ cmHg} / \text{molK}$), T is the absolute temperature (K), $\frac{dV}{dt}$ is the volumetric flow rate obtained from the flowmeter (cm^3 / s) and 22,414 is the number of cm^3 (STP) of penetrant per mole (Adewole, 2016).

Results and Discussion

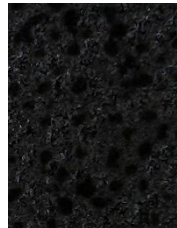
Morphological Evaluation



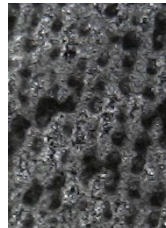
a) Cross-section of single layer membrane



b) Surface of single layer membrane



c) Surface of 3-layer membrane



d) Surface of 7-layer membrane



e) dispersed particles distribution in 3-layer membrane



f) dispersed particles distribution in 7-layer membrane

Figure 1. Optical microscopic images of membrane samples for different layers of printing membranes

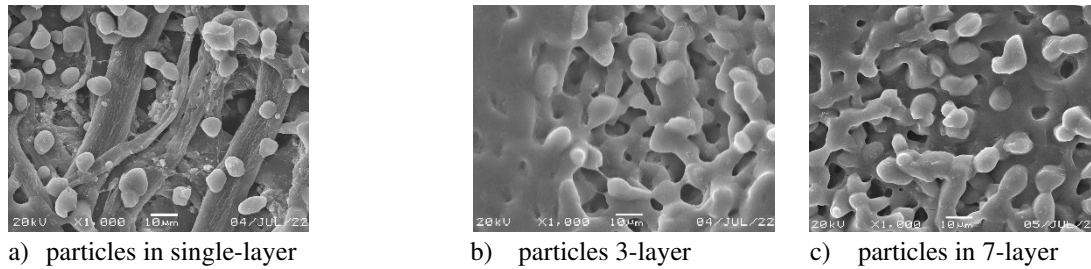


Figure 2 SEM images of membrane samples showing dispersed particles distribution for different layers of printed membranes.

The results of morphological studies of the fabricated membrane samples are shown in Figure 1 and Figure 2. The image from Figure 1 (a) clearly revealed the deposited layer on the cellulosic substrate. The deposited layer is black while the substrate is whitish in colour. The uniformly distributed patterns of particles are depicted in other figures (Figure 1 (b to f)). For example, Figure 1 (e) showed the particle distribution in the 3-layer mixed-matrix membrane. Similar patterns of particle distribution were found in single layer and 7-layer samples. This showed that print-assisted membrane fabricated technique can be used to make mixed-matrix membrane with dispersed phase uniformly distributed across the continuous phase. The results from optical microscope were complemented by the SEM results presented in Figure 2. From the images on this figure, it can be observed that the ink particles are well distributed within the chain of the cellulosic substrate.

XRD analysis

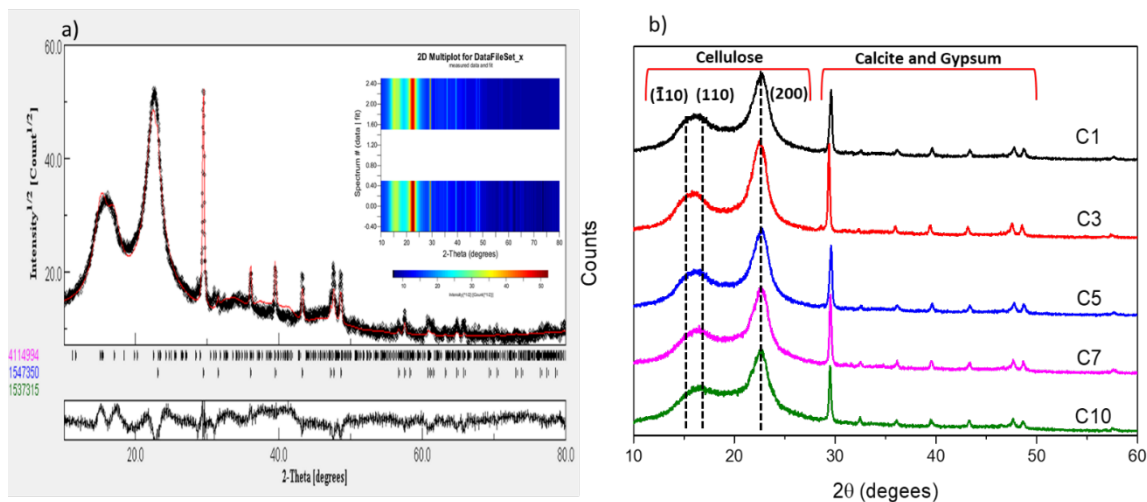


Figure 3 (a) the XRD pattern refinements using MAUD software for prepared samples, b) the XRD pattern of the as-prepared samples with different levels of ink deposition.

The as-prepared membrane samples were characterized by the X-ray diffraction (XRD) technique to investigate the structural and crystalline properties of the samples. The effect of the deposit ink layer on the quality of the cellulosic substrate was investigated. Figure 2(a) showed the XRD pattern refinements using MAUD software for the prepared sample. The sample showed a great agreement with three Cif cards references (4114994, 1547350 and 1537315) corresponding to cellulose ($C_6H_{10}O_5$), Calcite ($CaCO_3$), and Gypsum ($CaSO_4$) respectively. Figure 2 (b) present the XRD pattern of the as-prepared samples with different level of ink deposition. The main diffraction peaks representing the cellulose material are indicated by two diffraction peaks which are 110 and 200. The miller index (110) represents

the amorphous reflection which is located around 18.6° whereas the miller index (200) represents the cellulose crystalline peak found around 22.7° . The result presented in Figure 2 (b) showed that all prepared samples reflect the same diffraction pattern, however, the intensity ratio between crystalline and amorphous changed as the number of ink layers increased. Therefore, the degree of crystallinity index (CrI) of the membrane samples was calculated with the help of the equation suggested by (Segal *et al.*, 1959). The equation was used to calculate the CrI where I_{200} is the intensity of the cellulose crystalline peak and I_{110} is the intensity of the amorphous peak. The CrI result represented in Table 1 showed that crystalline property decreases with increasing number of layers deposited on the cellulosic substrate. This is expected to occur due to the penetration of ink particles into cellulose fibers thereby disrupting polymer chain packing and hence the crystallinity of cellulosic substrate.

Table 1. The relative degree of crystallinity index (CrI) values

Sample ID	C1	C3	C5	C7	C10
CrI	60.3	54.7	49.5	48.3	43.2

C1 (single layer), C3 (three-layer), C5 (five-layer) C7 (seven-layer), C10 (ten-layer)

FTIR analysis

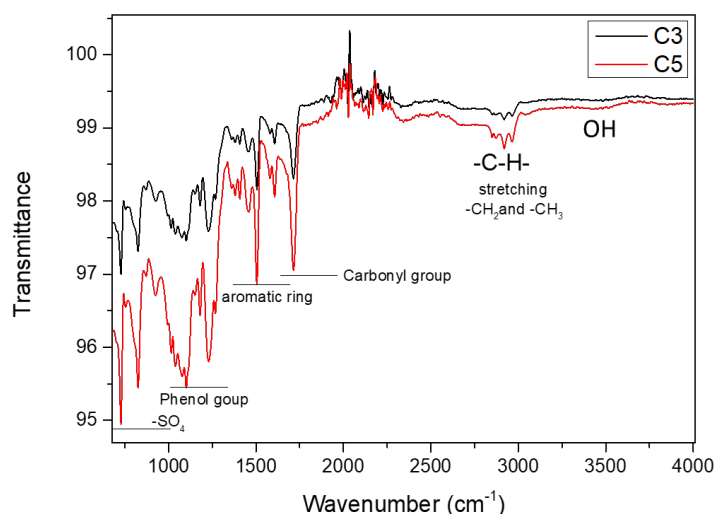


Figure 4: The FTIR spectrum of C3 and C5 samples.

Figure 3 showed the Fourier transform infrared (FTIR) spectrum of the as-prepared samples. The FTIR was used to identify the specific interaction of the functional groups present on the sample surface. The result was almost identical in terms of the presence of different functional groups with different samples. The result showed a strong peak near 610 cm^{-1} characteristic absorptions of the SO_4^{2-} group originating from calcium sulfate. The absorption peak at $1300\text{--}1000\text{ cm}^{-1}$ can be attributed to the phenol group mainly to C–O–H stretching from the carbohydrate group. The stretching vibration mode at 2894 cm^{-1} can be observed for C–H originating from bending vibrations of CH–COH at 1424 cm^{-1} , CCH–COH group at 1375 , 1345 , and 1316 cm^{-1} . Moreover, the C–O–C stretching at 1160 cm^{-1} has been recorded. Furthermore, weak peak bands related to OH groups at $3400\text{--}3200\text{ cm}^{-1}$ has been observed due to low levels of hydration. All peak observations can be attributed to ink-based material along with cellulose chemical structure.

Gas Permeation Test

The results of the permeation test on the membrane samples are shown in Figure 5 and Figure 6. The permeation tests were done for CO₂ and CH₄. In Figure 5, it can be observed that the permeability of both gases decreased with increase in the number of layers. An interesting observation is the rate of change of the permeability of each of the gases with respect to the number of layers. The rates of these changes are further elaborated on Table 2. The results on this table showed a gradual decrease of the permeability of the two gases at the beginning. The changes however became significant afterwards. For example, the permeability of CO₂ dropped by about 6% when the layer was increased by one. However, the permeability dropped by about 50% when the number of layers was increased by three. Though, similar behaviour was observed for CH₄ gas, however, the change observed is doubled that of CO₂. For instance, the permeability of CH₄ dropped by 12% when the layer was increased by 1 (this is double that of CO₂ which is 6%). Moreover, the drop in permeability was consistently observed to be higher for CH₄ than for CO₂. For both gases, the permeability decreased until the seventh layer after which the permeability was found to slightly increased. Contrary to what was observed before for samples between 0 and 7 layers, the increase in permeability was more for CO₂ than CH₄. For example, the permeability of CO₂ increased by about 61% while that of CH₄ increased by 27% (which is half of that of CO₂).

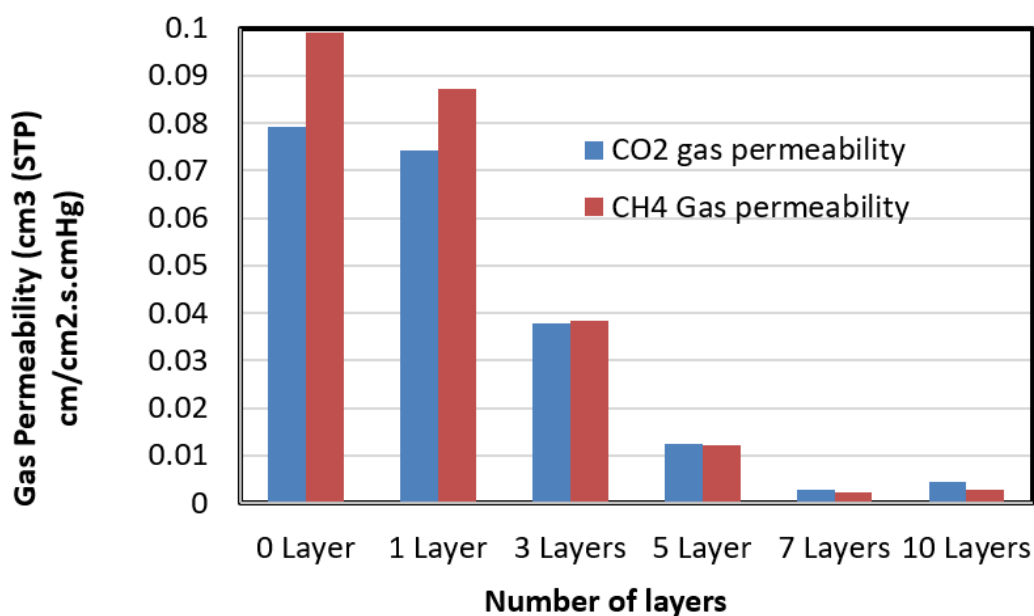


Figure 5: Gas permeability as function of the number of layers

Table 2 Change in permeability of gases with respect to number of layers

Sample	Change in permeability	
	CO ₂	CH ₄
0 Layer	0.00	0.00
1 Layer	-6.15	-11.89
3 Layer	-49.26	-56.13
5 Layer	-66.87	-68.59
7 Layer	-78.46	-81.30
10 Layer	60.71	27.03

The selectivity of the membrane samples to these two gases are shown in Figure 6. The behaviour observed for the permeability can also be found in the results of the selectivity. Samples with 0 to 2 layers can separate the two gases with CH₄ as permeate and CO₂ as retentate. Sample with 3 to 5 layers have selectivity of around one, which indicate that they cannot separate the two gases. The separation performance was found to be reversed for samples with more than 6 layers. Above six layers, the separation performance was found to increase with increase in number of layers. In addition, the membrane samples were able to separate the two gases with CO₂ as permeate and CH₄ as retentate. This means that the selectivity has been reversed.

The gas transport behaviours exhibited by these membrane samples can be explained based on the gas transport mechanism in porous membranes. The microscopic images of the membrane showed that these membranes fall in the category of porous membranes. Gas transport in porous membranes can be described using four different idealized mechanisms which include Knudsen diffusion, partial diffusion (capillary condensation), selective adsorption (surface diffusion), and molecular sieving (Williams and Koros, 2008; Ismail, 2010). In this work, two out of these mechanisms were clearly demonstrated. Gas transport in membrane samples with 0 to 2 layers were found to follow the Knudsen mechanism, whereas, in samples with 6 to 10 layers, the gas transport follows the molecular sieve mechanism. This means that the constrictions within the membrane with 0 to 2 layers were initially bigger than the sizes of both (CH₄ and CO₂). As the number of layers increased, the size of the constriction decreased until it approached the molecular dimension of the CO₂. In this manner, the membrane samples with number of layers from six layers and above were able to separate the gas mixture of CO₂ and CH₄ by allowing the passage of CO₂ molecules while restricting that of CH₄. Detailed of these two mechanisms are presented in (Williams and Koros, 2008).

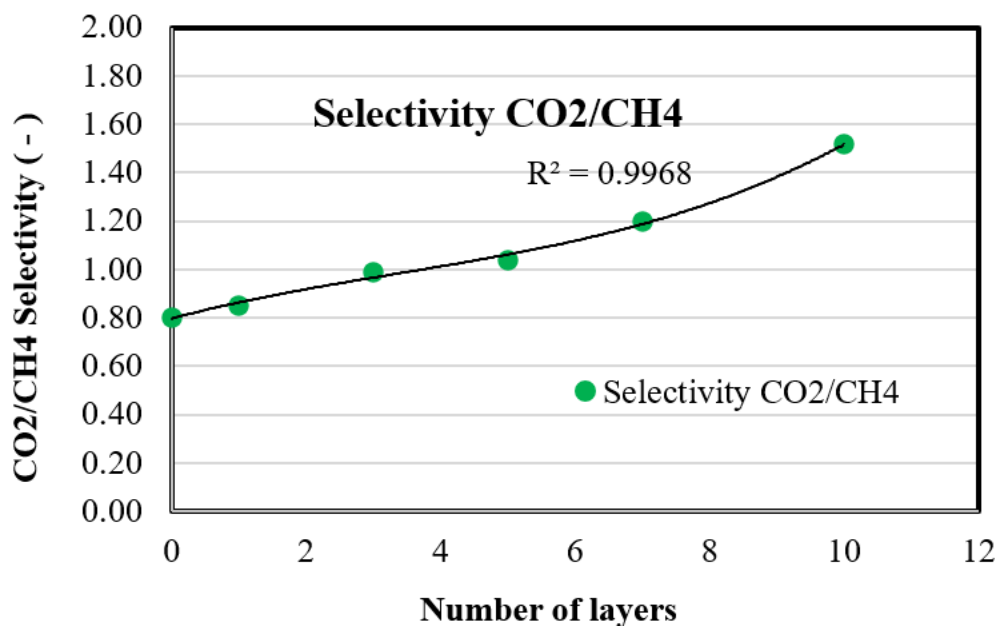


Figure 6. Changes in gas selectivity with respect to the number of layers

Conclusion

Flat sheet layer-by-layer mixed-matrix membrane samples were fabricated using a print-assisted technique to demonstrate how print-assisted technique can be used to achieve the spatial domain of process intensification. Membranes samples with different layers (from 0 to 10 layers) were fabricated using a LaserJet printer. The randomness and structured nature of the resulting mixed-matrix membrane was evaluated. The samples were analysed using scanning electron and optical microscopes, XRD, FTIR and permeation test with CO₂ and CH₄. The membrane samples were

found to demonstrate a mixed of gas transport mechanisms based on the number of layers. On a general note, the results of the performance tests showed that the fabricated membranes have some potentials for separating CO₂/CH₄ gas mixtures. The well-structured morphology of the fabricated membranes is an indication that the print-assisted method can be used to achieve the principle and domain of process intensification.

Acknowledgement

Authors would like to thank the Membrane Engineering Lab and Research and Graduate Studies Office of the International Maritime College Campus, National University of Science & Technology, Oman under the grant 2022/CRG07. We would also like to thank Mr Khalid S. Al Sa'idi for his help in drawing and Dr Muna Al Hinai for her help in facilitating the FTIR and XRD characterization.

References

- Adewole, J. K. *et al.* (2013) 'Current challenges in membrane separation of CO₂ from natural gas: A review', *International Journal of Greenhouse Gas Control*, 17. doi: 10.1016/j.ijggc.2013.04.012 Review.
- Adewole, J. K. *et al.* (2015) 'Comparative studies on the effects of casting solvent on physico-chemical and gas transport properties of dense polysulfone membrane used for CO₂/CH₄ separation', *Journal of Applied Polymer Science*, 132(27). doi: 10.1002/app.42205.
- Adewole, J. K. (2016) 'Transport properties of gases through integrally skinned asymmetric composite membranes prepared from date pit powder and polysulfone', *Journal of Applied Polymer Science*, 133(28). doi: 10.1002/app.43606.
- Adewole, J. K. and Ahmad, A. L. (2017) 'Polymeric membrane materials selection for high-pressure CO₂ removal from natural gas', *Journal of Polymer Research*, 24(5). doi: 10.1007/s10965-017-1231-6.
- Ahmad, A. L. *et al.* (2014) 'Preparation and gas transport properties of dual-layer polysulfone membranes for high pressure CO₂ removal from natural gas', *Journal of Applied Polymer Science*, 131(20). doi: 10.1002/app.40924.
- Drioli, E., Stankiewicz, A. I. and Macedonio, F. (2011) 'Membrane engineering in process intensification — An overview', 380, pp. 1–8. doi: 10.1016/j.memsci.2011.06.043.
- Holtbruegge, J., Wierschem, M. and Lutze, P. (2014) 'Chemical Engineering and Processing : Process Intensification Synthesis of dimethyl carbonate and propylene glycol in a membrane-assisted reactive distillation process : Pilot-scale experiments , modeling and process analysis', *Chemical Engineering & Processing: Process Intensification*, 84, pp. 54–70. doi: 10.1016/j.cep.2014.01.008.
- Ismail, A. F. (2010) '1.13 - Preparation of Carbon Membranes for Gas Separation', in Drioli, E. and Giorno, L. B. T.-C. M. S. and E. (eds). Oxford: Elsevier, pp. 275–290. doi: <https://doi.org/10.1016/B978-0-08-093250-7.00003-7>.
- Reay, D., Ramshaw, C. and Harvey, A. (2013a) 'Chapter 1 - A Brief History of Process Intensification', in Reay, D., Ramshaw, C., and Harvey, A. B. T.-P. I. (Second E. (eds) *Isotopes in Organic Chemistry*. Oxford: Butterworth-Heinemann, pp. 1–25. doi: <https://doi.org/10.1016/B978-0-08-098304-2.00001-8>.

Reay, D., Ramshaw, C. and Harvey, A. (2013b) 'Chapter 6 - Intensification of Separation Processes', in Reay, D., Ramshaw, C., and Harvey, A. B. T.-P. I. (Second E. (eds) *Isotopes in Organic Chemistry*. Oxford: Butterworth-Heinemann, pp. 205–249. doi: <https://doi.org/10.1016/B978-0-08-098304-2.00006-7>.

Segal, L. *et al.* (1959) 'An Empirical Method for Estimating the Degree of Crystallinity of Native Cellulose Using the X-Ray Diffractometer', *Textile research journal*, v. 29(10), pp. 786-794–1959 v.29 no.10. doi: 10.1177/004051755902901003.

Sitter, S., Chen, Q. and Grossmann, I. E. (2019) 'An overview of process intensification methods', *Current Opinion in Chemical Engineering*, 25, pp. 87–94. doi: <https://doi.org/10.1016/j.coche.2018.12.006>.

Stankiewicz, A. (2020) 'The Principles and Domains of Process Intensification', (March), pp. 23–28.

Stankiewicz, A. J. and Moulijn, J. A. (2000) 'Process Intensification: Transforming Chemical Engineering', *Chemical Engineering Progress*, 96, pp. 22–34.

Ulbricht, M. and Susanto, H. (2011) 'Porous Polymer Membranes by Manufacturing Technologies other than Phase Separation of Polymer Solutions', in *Membranes for Membrane Reactors: Preparation, Optimization and Selection*. Williams, P. J. and Koros, W. J. (2008) 'Gas Separation by Carbon Membranes', pp. 599–631.